UDK 539.3

V. D. Kubenko[1], G. Osharovich[2], M. V. Ayzenberg-Stepanenko[2]

IMPACT INDENTATION OF A RIGID BODY INTO AN ELASTIC LAYER. AXISYMMETRIC PROBLEM

An axisymmetric contact-impact problem is considered for an elastic layer subjected to normal indentation of a rigid body. An exact analytical solution is obtained in the case of a blunt shape of the indenter having a given velocity, and the stress pattern under multiple reflections is analyzed depending on the layer thickness. A numerical solution of the problem with arbitrary indenter shape is obtained on the basis of the simplified model of theory of elasticity having a single displacement coincident with the impact direction. The explicit finite difference algorithm is designed on the basis of the mesh dispersion minimization technique. Parametric analysis is presented of the stress pattern developed with time concerning to variations of irregular shapes of the indenter and its masses.

1. Introduction. This paper is the continuation to the axisymmetric case of the plane problem analyzed in [7]. The introduction presented in [7] could be practically completely replicated herein, as well as sited works within [7]. With analytical approaches in mind, we refer review [6] reflecting the multitude of studies of a body's impact interaction with elastic and liquid media, while numerical approaches (primarily the method of finite elements) can be found in review [17]. A generalizing monograph in the field of contact interaction [11] is devoted to the development of analytical approaches to the solution of problems about the action of impact on an elastic medium. In the common case, the indentation problem is formulated as a unsteady-state mixed initially-boundary elasticity problem with an unknown (temporally varying) boundary, which must be determined in the course of the solution. The problem statement includes:

- equations of dynamic deformation of the impacted solid;
- the equation of the indenter motion;
- the ratio presenting the resistive force (drag) as a function of contact stresses on *a priori* unknown contact surface;
- the equation connecting the contact zone size with the indenter displacement,
- the corresponding boundary and initial conditions.

The overwhelming majority of publications (at least of those in which analytical methods are used) are devoted to the problem of impact by rigid or deformable indenter against a halfspace that precludes the possibility of analyzing the waves reflected from the boundaries of the impacted solid. Studies of indenter interaction with solids of finite size are much less represented. Positing such a problem appears topical in the practical aspect as well – in particular, in view of the wide use of laminate materials in modern aircraft and shipbuilding. It is noteworthy that scale effect is among the determinant qualitative factors for problems of stresses and fracture in impact interaction (see e. g. [9, 10]): the structure element under impact loading is destroyed by stresses whose level is formed due to superposition of waves reflected from boundary surfaces. The classical Hertz theory of collision is known to be applicable in dynamics at large time values, i. e. after the wave processes have faded in the solid. The Saint-Venant wave theory of rod collision is well developed only for one-dimensional or quasi one-dimensional problems and does not take into account energy transfer in directions different from the impact one. The foresaid evaluates the motivation of the presented work devoted to the construction and investigation of more adequate models and methods for dynamic processes of indentation.

This paper, in similar to [7], consists of two parts: in the first one a precise analytical solution of the problem is built of the indentation with a constant

impact velocity of an smooth shape axisymmetric rigid body into an elastic layer. The dynamic process is determined by the superposition of the initial and reflected waves with different physical and mechanical characteristics of the layer material.

The computer solution obtained in the second part is built on the basis of the simplified model of theory of elasticity with a single displacement introduced in [12] and used in a set of dynamical problems (see references to [7]), in which the displacement coincident with the impact direction predominates. In the model, the two-dimensional character remains of the process under consideration, while instead of the traditional equations of theory of elasticity axial stresses are eliminated. The explicit finite difference algorithms are used together with the mesh dispersion minimization (MDM) approach, resulting in precise calculations of discontinuities. The MDM, originally created in [15] for one-dimensional hyperbolic equations and upgraded in [1–3, 5, 13] for computation of wave and fracture processes in elastic and hydro-elastic systems, was for the first time applied to the two-dimensional contact-impact problem in [7]. The MDM technique is based on a generalized concept of the Courant condition that relates mesh parameters to wave velocity, which reflects properties of the material at hand. Difference presentation of original differential equations exhibits some typical domains of influence, and the idea behind MDM is to properly adjust these domains so as to improve convergence. To this end, phase velocities of high-frequency components of the continuous model have to be considered, and the mesh to be set so that the propagation velocities in the discrete model approximate the former as closely as possible. An important technical advantage of MDM is that it utilizes the same mesh for both high-gradient and smoothed components of solution. A satisfactory correspondence of analytical and computer solutions opens the way for using the latter to solve contact-impact problems, in which the indenter has an irregular shape (see [7]).

In this paper, the parametric analysis is presented of the stress pattern and the drag developed with time concerning to variations of indenter shapes and masses.

2. Problem statement. A rigid indenter reaches the surface of elastic layer $z = 0$ at time $t = 0$ and begins to press into it. The pressing-in process is specified by the indenter's velocity $V_0(t)$ perpendicular to the layer's surface. The impact velocity is assumed to be much less than that of the elastic waves in the layer, while the penetration depths are insignificant. This enables to use the formulation of a linear problem of theory elasticity with the boundary conditions remaining valid for the undisturbed layer surface. We refer the layer to polar coordinates r, z $(-\infty < r < \infty,\ 0 \le z \le h)$, so that radial coordinate r is directed along the free surface and axis z into the layer (Fig. 1). The indenter surface is defined by rotation (with respect to axis z) of given curve $z = f(r)$. We introduce dimensionless notations

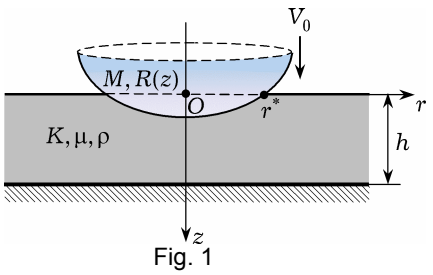

Fig. 1

$$\bar{r} = \frac{r}{R}, \qquad \bar{z} = \frac{z}{R}, \qquad \bar{u}_i = \frac{u_i}{R}, \qquad \bar{t} = \frac{c_0 t}{R}, \qquad \bar{V}_0 = \frac{V_0}{c_0},$$

$$\bar{\sigma}_{ij} = \frac{\sigma_{ij}}{K}, \quad i,j = r,z, \qquad \beta = \frac{c_s}{c_0}, \qquad \alpha = \frac{c_p}{c_0}, \qquad b = \frac{\beta}{\alpha},$$

$$\bar{w}_0 = \frac{w_0}{R}, \qquad c_p = \left(\frac{K + 4/3\mu}{\gamma}\right)^{1/2}, \qquad c_s = \left(\frac{\mu}{\gamma}\right)^{1/2}, \qquad c_0 = \left(\frac{K}{\gamma}\right)^{1/2}. \qquad (1)$$

The line above the notations will be omitted below. Here R is the characteristic linear dimension of the indenter, V_0 is its impact velocity, w_0 is its displacement counted from the undisturbed surface of the upper layer; c_p and c_s are, respectively, velocities of longitudinal and shear waves in the layer material, γ is its density; K is its uniform compression modulus, λ, μ are Lame's constants; u_j are components of the displacement vector and σ_{ij} are components of the stress tensor.

The behavior of the elastic medium is described by potentials Φ and Ψ, which in the case of an axisymmetric problem satisfy wave equations

$$\Delta\Phi = \frac{1}{\alpha^2}\frac{\partial^2\Phi}{\partial t^2}, \qquad \Delta\Psi = \frac{1}{\beta^2}\frac{\partial^2\Psi}{\partial t^2}, \qquad \Delta \equiv \frac{\partial^2}{\partial r^2} + \frac{1}{r}\frac{\partial}{\partial r} + \frac{\partial^2}{\partial z^2}. \tag{2}$$

Potentials are connected with displacements and stresses by relationships

$$u_r = \frac{\partial\Phi}{\partial r} + \frac{\partial^2\Psi}{\partial r\partial z}, \qquad u_z = \frac{\partial\Phi}{\partial z} - \frac{\partial^2\Psi}{\partial r^2} - \frac{1}{r}\frac{\partial\Psi}{\partial r},$$

$$\sigma_{zz} = (1-2b^2)\frac{\partial^2\Phi}{\partial t^2} + 2\beta^2\left(\frac{\partial^2\Phi}{\partial z^2} - \frac{\partial^3\Psi}{\partial r^2\partial z} - \frac{1}{r}\frac{\partial^2\Psi}{\partial r\partial z}\right),$$

$$\sigma_{rr} = (1-2b^2)\frac{\partial^2\Phi}{\partial t^2} + 2\beta^2\left(\frac{\partial^2\Phi}{\partial r^2} + \frac{\partial^3\Psi}{\partial r^2\partial z}\right),$$

$$\sigma_{rz} = 2\beta^2\frac{\partial}{\partial r}\left(\frac{\partial\Phi}{\partial z} + \frac{\partial^2\Psi}{\partial z^2} - \frac{1}{2\beta^2}\frac{\partial^2\Psi}{\partial t^2}\right). \tag{3}$$

The bluntness of the indenter face and a relatively small indentation deep allow us boundary conditions to be formulated on undisturbed halfspace surface $z = 0$. The indenter surface in current time moment t is described by the following way:

$$z_{\text{ind}} = w_0(t) - f(r), \qquad w_0(t) = \int_0^t V_0(\tau)\,d\tau, \qquad f(0) = 0. \tag{4}$$

Following to the accurate formulation of the linear problem, radius of the contact zone, $r^*(t)$, is obtained from the kinematical condition below with deformation of the layer free surface taken into account:

$$w_0(t) - f(r) - u_z(t,r,0) = \begin{cases} 0, & 0 \le r < r^*(t), \\ < 0, & r > r^*(t). \end{cases} \tag{5}$$

The initial conditions for wave potentials are zero. The boundary conditions of the problem are formulated on front, $z = 0$, and back, $z = h$, surfaces. Boundary conditions at $z = 0$ are: equality of indenter and normal layer displacements inside the interface, absence of normal stress σ_{zz} outside of it, and absence of tangential stresses σ_{rz}:

$$u_z\big|_{z=0} = w_0(t), \qquad r \le r^*,$$

$$\sigma_{zz}\big|_{z=0} = 0, \qquad r > r^*,$$

$$\sigma_{rz}\big|_{z=0} = 0. \tag{6}$$

Besides, it is necessary to see that σ_{zz} in the interface should remain compressing at all the period of interaction:

$$\sigma_{zz}\big|_{z=0} < 0, \qquad r \le r^*. \tag{7}$$

Normal displacements and shear stresses are zero at the layer back surface

$$u_z = 0, \qquad \sigma_{rz} = 0, \qquad z = h. \tag{8}$$

The boundaries of the contact zone will be the intersection points of the body indenting contour $r^*(t)$ and plane $z = 0$; if the surface of the moving body in the space of variables r, z, t is set by equation $z = F(t, r)$, the contour indicated points $r^*(t)$ is to be obtained from equation

$$F(t, r) = 0. \tag{9}$$

System (1)–(9) formulates the problem of indenter and layer interaction at the given impact velocity.

3. Analytical solution. This section is based on the problem solving technique presented in [8]. The formulated problem admits an analytical solution on the condition that the indenter contour is a sufficiently smooth, gently changing curve. Let the flatness of the indenter be such that at small times of interaction the mentioned above contour $r^*(t)$ under conditions (4) moves along the surface $z = 0$ with velocity exceeding that of the elastic waves. As a result the latter do not emerge on the free layer surface, and conditions on boundary $z = 0$ are

$$\left.\frac{\partial u_z}{\partial t}\right|_{z=0} = H(r^* - r)V_0(t) = V_0(t, r), \qquad \sigma_{rz}\big|_{z=0} = 0. \tag{10}$$

Here $H(\cdot)$ is the Heaviside step function. The condition on the layer backing remains unchanged

$$u_z\big|_{z=h} = 0, \qquad \sigma_{rz}\big|_{z=h} = 0. \tag{11}$$

The solution to be obtained here, apart from its independent significance, also serves below to test the numerical algorithm.

Following to [8] we use the Laplace integral transform in time (parameter s, upper index L) and the Bessel integral transform along the radial coordinate (parameter ξ, upper index B):

$$f^L(s) = L\{f(t)\} = \int_0^\infty e^{-st} f(t)\, dt,$$

$$f(t) = L^{-1}\{f^L(s)\} = \frac{1}{2\pi}\int_{\delta-i\infty}^{\delta+i\infty} e^{ts} f^L(p)\, dp,$$

$$f^B(\xi) = B\{f(r)\} = \int_0^\infty f(r)\, r J_0(r\xi)\, d\xi,$$

$$f(r) = B^{-1}\{f^B(\xi)\} = \int_0^\infty f^B(\xi)\, \xi J_0(r\xi)\, d\xi.$$

Here J_0 is the cylindrical function of the first kind. In the image space the wave equations will take the form (with zero initial and necessary boundary conditions taking into account):

$$\frac{\partial^2 \Phi^{LB}}{\partial z^2} - \left(\frac{s^2}{\alpha^2} + \xi^2\right)\Phi^{LB} = 0, \qquad \frac{\partial^2 \Psi^{LB}}{\partial z^2} - \left(\frac{s^2}{\beta^2} + \xi^2\right)\Psi^{LB} = 0,$$

$$\frac{\partial \Phi^{LB}}{\partial z} + \frac{\partial^2 \Psi^{LB}}{\partial z^2} - \frac{s^2}{\beta^2}\Psi^{LB} = \begin{cases} \frac{1}{s} f^{LB}(s, \xi), & z = 0, \\ 0, & z = h, \end{cases}$$

$$\frac{\partial \Phi^{LB}}{\partial z} + \frac{\partial^2 \Psi^{LB}}{\partial z^2} - \frac{s^2}{2\beta^2}\Psi^{LB} = 0, \qquad z = 0, \qquad z = h, \tag{12}$$

where $f^{LB}(s, \xi)$ is the double Laplace – Bessel image of function $V_b(r, t)H\big(t - r^*(t)\big)$.

The general solution of wave equations is the following:

$$\Phi^{LB} = A_+ e^{-\frac{z}{\alpha}\sqrt{s^2+\alpha^2\xi^2}} + A_- e^{\frac{z}{\alpha}\sqrt{s^2+\alpha^2\xi^2}},$$

$$\Psi^{LB} = B_+ e^{-\frac{z}{\beta}\sqrt{s^2+\beta^2\xi^2}} + B_- e^{\frac{z}{\beta}\sqrt{s^2+\beta^2\xi^2}}. \qquad (13)$$

Then functions $A_\pm(s,\xi)$, $B_\pm(s,\xi)$ are obtained after satisfying the remaining boundary conditions:

$$A_\pm = -\alpha f^{LB}(s,\xi)\frac{(s^2+2\beta^2\xi^2)e^{\pm\frac{h}{\alpha}P}}{s^3\sqrt{s^2+\alpha^2\xi^2}\left(e^{\frac{h}{\alpha}P} - e^{-\frac{h}{\alpha}P}\right)},$$

$$B_\pm = -2\beta^2 f^{LB}(s,\xi)\frac{e^{\pm\frac{h}{\beta}S}}{s^3\left(e^{\frac{h}{\beta}S} - e^{-\frac{h}{\beta}S}\right)}.$$

Now one can obtain the following expression for the image of normal stress σ_{zz}^{LF}:

$$\sigma_{zz}^{LB}(s,\xi,z) =$$

$$= -\alpha f^{LB}(s,\xi)\left[\frac{(s^2+2\beta^2\xi^2)^2}{s^3\sqrt{s^2+\alpha^2\xi^2}}\left(\sum_{m=0}^{\infty} e^{-(2mh+z)P} + \sum_{m=0}^{\infty} e^{-[2(m+1)h-z]P}\right) - \right.$$

$$\left. - \frac{4\beta^3}{\alpha}\frac{\xi^2\sqrt{s^2+\beta^2\xi^2}}{s^3}\left(\sum_{m=0}^{\infty} e^{-(2mh+z)S} + \sum_{m=0}^{\infty} e^{-[2(m+1)h-z]S}\right)\right]. \qquad (14)$$

Our problem is to reverse expression (14) with respect to integral transforms. To this end, we restrict analytical results by obtaining normal stresses in the axis $z(r=0)$ in the case of a parabolic surface of the indenter moving with a constant velocity V_0. Then it can be seen that function $f(r,t)$ and its transform are the following:

$$f(t,r) = V_0 H(kt - r^2), \qquad f^{LB}(s,\xi) = V_0\frac{k}{2s^2}e^{-\xi^2\frac{k}{4s}}, \qquad k = 2V_0. \qquad (15)$$

Omitting details of the reversion technique (see [8]) we present the final expression of the above-mentioned stresses

$$\sigma_{zz}(t,z)\big|_{r=0} =$$

$$= -\alpha V_0\left\{\sum_{m=0}^{\infty} H(t-Z_{m1})\frac{\left(1+8\frac{\beta^2}{k^2}T_{m1}(t,z)\right)^2}{\sqrt{1+4\frac{\alpha^2}{k^2}T_{m1}(t,z)}}\left(1-\frac{2\alpha^2 Z_{m1}(z)}{R_{m1}(t,z)}\right) + \right.$$

$$+ \sum_{m=0}^{\infty} H(t-Z_{m2})\frac{\left(1+8\frac{\beta^2}{k^2}T_{m2}(t,z)\right)^2}{\sqrt{1+4\frac{\alpha^2}{k^2}T_{m2}(t,z)}}\left(1-\frac{2\alpha^2 Z_{m2}(z)}{R_{m2}(t,z)}\right) -$$

$$- \frac{16\beta^3}{\alpha k^2}\sum_{m=0}^{\infty} H(t-Z_{m3})T_{m3}(t,z)\sqrt{1+4\frac{\beta^2}{k^2}T_{m3}(t,z)}\left(1-\frac{2\beta^2 Z_{m3}(z)}{R_{m3}(t,z)}\right) -$$

$$\left. - \frac{16\beta^3}{\alpha k^2}\sum_{m=0}^{\infty} H(t-Z_{m4})T_{m4}(t,z)\sqrt{1+\frac{4}{k^2}\beta^2 T_{m4}(t,z)}\left(1-\frac{2\beta^2 Z_{m4}(z)}{R_{m4}(t,z)}\right)\right\}, \qquad (16)$$

where

$$T_{mj}(t,z) = kt + 2Z_{mj}^2\alpha^2 - Z_{mj}R_{mj}(t,z),$$

$$R_{mj}(t,z) = \sqrt{k^2 + 4\alpha^2 kt + 4\alpha^4 Z_{mj}^2}, \qquad j = 1,\ldots,4,$$

$$Z_{m1}(z) = \frac{2mh + z}{\alpha}, \qquad Z_{m2}(z) = \frac{(2m+1)h - z}{\alpha},$$

$$Z_{m3}(z) = \frac{2mh + z}{\beta}, \qquad Z_{m4}(z) = \frac{(2m+1)h - z}{\beta}.$$

Obtained formula (16) is a precise analytical expression for normal stress $\sigma_{zz}(t,z)$ at arbitrary point of the layer on axis z. It consists of four infinite sums: each m-th item of the first (second) sum represents the m-th expansion wave reflected from the front (back) surface of the layer; each m-th item of the third (fourth) sum represents the m-th shear wave reflected from the front (back) surface of the layer. Keeping a finite number of items N in these sums, we obtain the value of stress with account taken of N reflections, which is the exact solution of the considered problem on the time interval $\frac{z}{\alpha} < t < \frac{2Nh + z}{\alpha}$.

In Fig. 2*a* normal stresses $\sigma_{zz}(0,z)$ at the axis $r = 0$ obtained with formula (16) are depicted. The indenter shape is given by expression (15), $V_0 = 0.1$. Parameters of the layer material are $\alpha = 1$, $\beta = 0.5$, the layer thickness is $h = 1.0$.

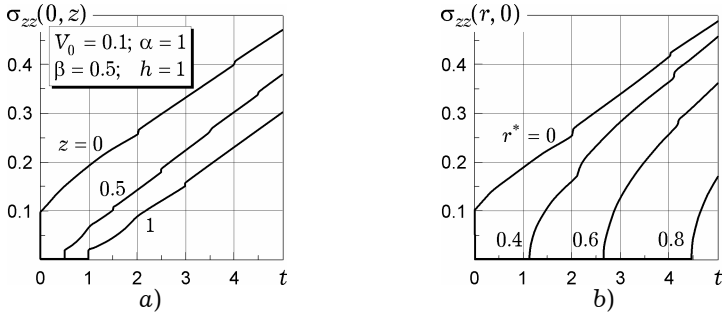

Fig. 2. Parabolic indenter vs. an elastic layer: *a*) analytical solution for normal stresses $\sigma_{zz}(0,z)$ in cross-sections $z = 0, 0.5, 1.0$ vs. time; *b*) numerical solution for normal stresses $\sigma_{zz}(0,z)$ at the interface $z = 0$, vs. time for $r^* = 0, 0.4, 0.6$ and 0.8.

As it can be seen, $\sigma_{zz}(0,0) = V_0$ at the initial moment of interaction, once after that $\sigma_{zz}(0,0)$ monotonically increases with time up to the moment of incoming the first reflected wave. Then a step-wise pattern of σ_{zz} is realized due to multiple reflections. The each successive discontinuity at the front of reflection waves is decreased in comparison with general rise of stresses. Average values of $\sigma_{zz}(0,z)$ linearly increase with time and inversely proportional to the general rigidity of the layer (or, it the same, to the layer thickness). The analogue pattern was also obtained in plane case [7]. Note that additional results calculated with (16) depending on parameters of layer material and its thickness are presented in [8].

4. Numerical solution. In this section, results of computer simulations are presented of the considered problem for some irregular shapes of the indenter having sharp edges (i.e. with discontinuities in the shape curvature), which result in singular stresses arising in the indentation process. To the best of the present authors' knowledge, closed analytical solutions are absent for the considered impact-contact problems.

Recall that in the case of the plane problem the MDM finite difference solution is obtained in [7] on the basis of the Rachmatullin simplified model of theory of elasticity with a singe displacement [12]. The simplification are based on corresponding physical-geometrical assumptions. The solution obtained by this way requires of a purposeful comparison with the precise model of theory of elasticity and evaluation of a discrepancy.

The model declares the following inequalities and consequences for stress components:

$$\frac{\partial u_z}{\partial z} \gg \frac{\partial u_r}{\partial r} \quad \Rightarrow \quad \sigma_{zz} \sim c_p^2 \gamma \frac{\partial u_z}{\partial z},$$
$$\frac{\partial u_z}{\partial r} \gg \frac{\partial u_r}{\partial z} \quad \Rightarrow \quad \sigma_{rz} \sim c_p^2 \gamma \left(\frac{\partial u_z}{\partial r} + \frac{u_z}{r} \right). \tag{17}$$

As a result, displacement u_r is eliminated in equations of theory of elasticity, and in the obtained by this way modified axisymmetric problem following (single) governing equation remains with respect to normal displacement $u(r,z,t) \equiv u_z(r,z,t)$:

$$\frac{\partial^2 u}{\partial t^2} = \frac{\partial^2 u}{\partial z^2} + c_s^2 \left(\frac{\partial^2 u}{\partial r^2} + \frac{1}{r} \frac{\partial u}{\partial r} \right). \tag{18}$$

Here and below c_p and γ are used as measurement units. Besides, we postulate zero initial conditions and the following (modified) boundary conditions:

$$z = 0: \qquad \dot{u} = V_0(r,t), \quad r \le r^*, \quad \frac{\partial u}{\partial z} = 0, \quad r > r^*,$$
$$z = h: \qquad u = 0. \tag{19}$$

The indenter motion is calculated by the following way:

$$\ddot{w}_0(t) = \frac{F(t)}{M}, \qquad F(t) = \frac{1}{2} \int_0^{r^*} \sigma(r,0)\, r\, dr,$$
$$w_0(0) = 0, \qquad \dot{w}_0(0) = V_0, \qquad V(t) = \dot{w}_0(t). \tag{20}$$

In this simplified formulation neither axial displacement u_r nor axial stress σ_{rr} are determined, and component $\partial u_r / \partial z$ of shear stresses is also absent. Because a single displacement is postulated, shear boundary conditions at $z = 0$ and $z = h$ are not required here. As was shown in [7] the considered model is turned be in good correspondence with the conventional theory of elasticity. Below we compare the results obtained by this model in the axisymmetrical case with the analytical solution presented above, in Section 3. The indirect justification for application of this simplified model to the considered problem can be found in the fact that it correctly described the qualitative stress pattern obtained for the analytical solution (see Fig. 2) and has controlled quantitative divergence.

As in [7], a reason to using the simplified model is the methodological one: the explicit difference algorithm presented below and applied to the model allows front discontinuities and singular components of the solution to be calculated without parasite effects of the mesh discretization. Note, in connection with this, that in a lot of computer algorithms designed to contact-impact problem solving the question how to accurate describe wave fronts and high gradients of solutions remains open. To eliminate parasite oscillations arising in front vicinities appeared in explicit and implicit difference algorithms including those used in commercial hydro-codes (see, for example [4, 16, 17]), the so-called artificial viscosity is introduced. This technique permits the parasite oscillations to be significantly decreased, however, at the same time it results in spreading front discontinuities. In problems similar to the discussed here,

the wave pattern is formed by multiple reflections, and, with their accurate description in mind, the artificial viscosity is turned be unacceptable. Thus, mesh dispersion, rather than the approximation problem, is the main obstacle for accurate calculations of contact-impact problems by explicit algorithms. Beginning from [15], the MDM algorithms were designed and successfully realized in [1–3, 5, 13] for diverse 1D wave propagation problems an related applications, while to the best of the present authors' knowledge MDM algorithms for calculating 2D wave processes have been designed for the first time in [7] to analyze a plane contact-impact problem. In this work, MDM algorithms elaborated in [7] are adapted for the axisymmetric problem formulated above.

In the computer model we introduce difference mesh steps Δt, Δz and Δr for discrete.

Approximation of spatial and temporal coordinates: $t = k\Delta t$, $z = j\Delta z$ and $r = i\Delta r$, where $k = 0,\dots,K$, $i = 0,\dots,I$, and $j = 0,\dots,J$, $J = h/\Delta z$. Integer K and I will be chosen from the condition of absence of influence of artificial boundary $x = I\Delta x$ on the $\{r, z, t\}$-domain of interest. For derivations from (18) we use the following discretizations:

$$\ddot{u} \sim (u_{j,i}^{k+1} - 2u_{j,i}^{k} + u_{j,i}^{k-1})\frac{1}{(\Delta t)^2},$$

$$u''_{zz} \sim (u_{j+1,i}^{k} - 2u_{j,i}^{k} + u_{j-1,i}^{k})\frac{1}{(\Delta z)^2},$$

$$u'_{r} \sim (u_{j+1,i}^{k} - u_{j-1,i}^{k})\frac{1}{2\Delta z},$$

$$u''_{rr} \sim (U_{j,i+1}^{k} - 2U_{j,i}^{k} + U_{j,i-1}^{k})\frac{1}{(\Delta r)^2}, \qquad (21)$$

where

$$U_{j,i}^{k} = \frac{1}{4}(u_{j+1,i}^{k} + 2u_{j,i}^{k} + u_{j-1,i}^{k}).$$

In scheme (21), the first three approximations are conventional, which are used in the explicit algorithm, while the forth one is the MDM representation of $U_{j,i}^{k}$. As it can be seen, in the discrete analog of (18) built with (21), the accuracy level of difference approximations, $(\Delta t)^2 + (\Delta z)^2 + (\Delta x)^2$, remains the same as in a conventional case with postulated equality $U_{j,i}^{k} \equiv u_{j,i}^{k}$.

In figures below, we present results calculated by model (18), (19) with approximation (21). Examples of calculation illustrate unsteady-state stress patterns developed in a halfspace or in a finite thickness layer under impact indentation of solid punches of various shapes and masses. The layer thickness is taken $h = 1$, while the case of a halfspace ($h \sim \inf$) thickness $h = H$ is taken so that waves reflected from the layer backing $z = H$ are not detected in the region, in which calculation results are analyzed. We consider cylindrical, parabolic, conical and mixed (the cylinder with parabolic or conical heads) indenter shapes. In the case of a cylindrical indenter with various head shapes the length unit is the cylinder radius ($R = 1$). Units of the velocity, stress and density are c_p, α, and γ, respectively. The problem linearity allows the initial impact velocity, V_0, to be taken equal to c_p ($\bar{V}_0 = 1$). In examples without the natural size unit (unbounded in the radial direction paraboloid and cone indenters interacted with a halfspace), the length and time are normalized by steps of the difference mesh. All examples are calculated

with $\beta = 0.5$. Results shown in Figs. 3–7 corresponds to an infinite indenter mass ($M \sim \inf$); in this case the initial impact velocity ($V_0 = 1$) remains constant as in the analytical solution above. Calculations with the finite indenter mass (Figs. 8, 9) were conducted for the case of a cylindrical punch with the plane head indented into a halfspase.

Preparatory to the description of computer results we must premise with the following general notation. The action of indenters having singular head shapes (by another words, punches with edges) results in a sharp bend in the front surface and in singular stresses developed in the edge vicinity. The used here linear deformation model is not suitable for description such singularities, and the mentioned results can be considered as a first approximation for a nonlinear case. Note also that discrete computer models determine the average shear angles and average stresses over the area of the spatial step. This circumstance is taken into account below in the analysis of numerical solutions.

First, with the aim to compare analytical and numerical solutions, an indenter with the parabolic shape is considered. In Fig. 2*b* normal stresses $\sigma_{zz}(r,0)$ at the interface $z = 0$ are depicted vs. time. All the parameters are the same that taken in the analytical solution shown in Fig. 2*a*: $h = 1$, the indentation velocity $V_0 = 0.1$, the parameter of the paraboloid curvature is 0.2. Steps of the difference mesh are $\Delta r = \Delta z = \Delta t = 0.001$.

Comparison of analytical and computer solutions (upper curves in Fig. 2*a* and Fig. 2*b* respectively) shows a good qualitative correspondence of this two approaches. Quantitative difference is that stress amplitudes in computer solution turns out be higher than analytical those, the convergence increases with time and its maximal value behaves about of ~ 6% at the vicinity of $t \sim 5$. As calculation show, in cases of relatively low β this convergence is more significant and increases with decrease in β.

In the above-considered case ($r^* = \sqrt{2tV_0}$, $V_0 = 0.1$), velocity of the interface $\dot{r}^*$ is supersonic at $t < 0.2$, transonic at $t = 0.2$ ($r^* = 0.2$), and subsonic at $t > 0.2$. In the subsonic zone, r^* rapidly decreased with time, and a part of the surface $z = 0$, $r > r^*$ is disturbed before the indenter pressing in (due to action of waves, radiated by a part of the surface ($z = 0$, $r > r^*$). In according with this, the contact at the interface is realized with a some delay. Time moments of the indenter incoming to several sections of surface $z = 0$ can be fixed at the beginning of curves: $t = 1.13$ ($r^* = 0.4$), $t = 2.66$ ($r^* = 0.6$), and $t = 4.45$ ($r^* = 0.8$). One can see that front discontinuities of reflected waves are decreased with increase in r.

In Fig. 3*a* the geometry of the cylindrical indenter with a paraboloid head is shown, while in Fig. 3*b* normal stresses $\sigma_{zz}(r,0)$ are depicted vs. time at the interface $z = 0$. Parameters of the indenter are: mass $M \sim \inf$, paraboloid constant $k = 2.5$. Curves correspond to $r = 0, 0.5, 0.75, 0.90, 0.95$, respectively, and curve for stresses $0.5 \cdot \sigma_{zz}(1,0)$ at $r = 1$ is depicted in Fig. 3*b*. It can be seen that in this case of a relatively shallow head of the indenter, stresses $\sigma_{zz}(r,0)$ are slightly changed in region $0 < r < 0.75$, therefore amplitudes of reflected waves are revealed more significant than those shown in Fig. 2 for the case a curved shape, and vice versa: in the vicinity of the punch edge $r = 1$, stresses $\sigma_{zz}(r,0)$ are rapidly changed, while the relative values of reflection fronts are decreased.

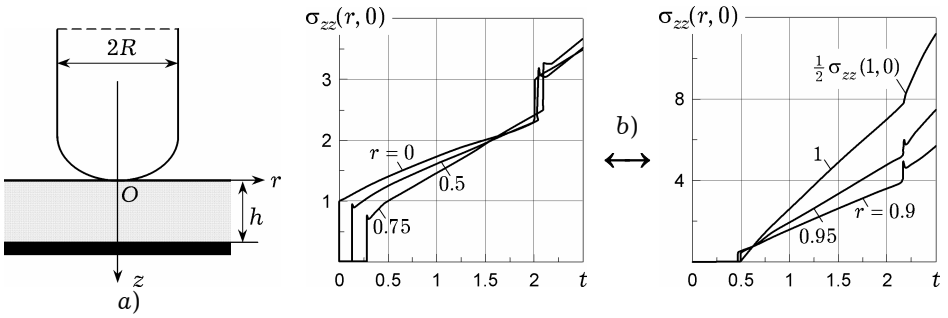

Fig. 3. Cylindrical indenter with a paraboloid head (curvature factor – $k = 2.5$) vs. an elastic layer: *a*) geometry of the problem; *b*) normal stresses $\sigma_{zz}(r,0)$ at the interface vs. time for $r = 0, 0.5, 0.75, 0.9$ and 0.95.

In Figs. 4 and 5 calculation results are shown related to indentation of a cylindrical punch ($M \sim \inf$) with a plane face. In Fig. 4, radial distributions are depicted of normal stresses σ_{zz} at the surface $z = 0$ of a halfspace and in vertical cross-sections $z = 0.05$, 0.1 and 1.0 at moments of time $t = 0.05$, 1.0 and 2.0. Presented results show a singular character of stresses at the surface $z = 0$ and their near-surface pattern.

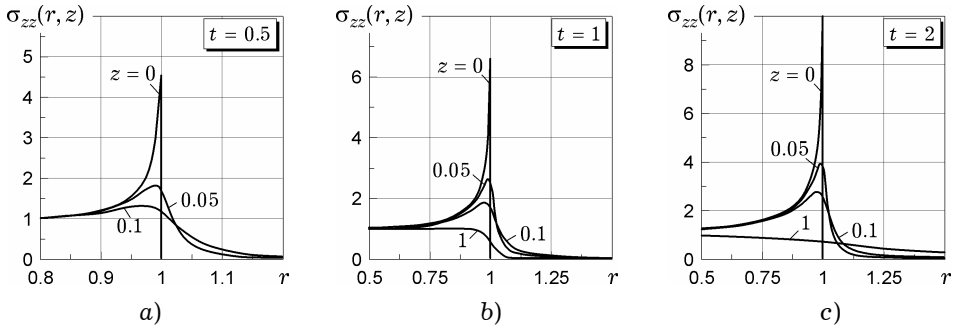

Fig. 4. Cylindrical indenter with a flat head vs. an elastic halfspace: distributions of normal stresses $\sigma_{zz}(r,z)$ along the radial coordinate at time moments $t = 0.05$, 1.0 and 2.0; curves corresponds to the interface $z = 0$, and cross-sections $z = 0.05, 0.1$ and 1.0.

Stresses $\sigma_{zz}(r,0)$ and drag F (normalized to the cylinder square) in the case $h = 1$ are shown in Fig. 5*a*. Curves correspond to $r = 0$, 0.5, 0.9, 0.95, 0.99 and 1.00. Due to the chosen scale, curves for $r = 0$ and $r = 0.5$ are weakly differed.

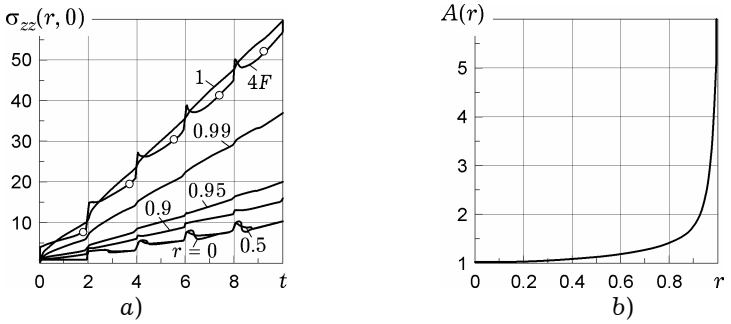

Fig. 5. Cylindrical indenter with a flat head vs. an elastic layer: *a*) drag F and normal stresses $\sigma_{zz}(r,0)$ vs. time, curves correspond to $r = 0, 0.5, 0.9, 0.95, 0.99$ and 1.00; *b*) factor $A(r)$ for linear dependence on time of normal stresses at the interface.

Analysis of the above-presented data results in the following conclusions:

– a singularity-caused strong non-uniformity of stresses distributed along the interface is preserved for all the process time;

– shear waves induced from the singularity $r = 1,\ z = 0$ are not practically influenced in stresses $\sigma_{zz}(r,z)$ in the singularity region, while they can be watched at the vicinity of the axis ($\sim r \le 0.5$ in presented figures), where the effect of convergent shear waves is maximal;

– the value of the relative contribution of discontinuities in stress (and drag) amplitudes caused by incoming fronts of reflected waves decrease with time in the almost all interface excluding the small vicinity of axis $r = 0$;

– the dependence of stresses (and drag) is approached to be linearly proportional to time.

With the last conclusion in mind, we obtain time asymptotes $\sigma_{zz}(r,0) \sim$ $\sim A(r)t$. In Fig. 5*b* this dependence is depicted. The similar factor for the drag, A_d, is 1.5. Note, that this value obtained in the plane problem [7] (with the same parameters) was $A_d \sim 1$ that allowed the following rough practical estimation to be proved: the drag value can be obtained on the basis of the simplest 1D «spring model»: the layer can be described by an inertionless spring having an effective rigidity of the vertical cylinder with the radius equals to the punch radius. Thus, a detectable difference exists for resistance to indentation of plane and axisymmetric punches, the latter is ~ 1.5 times greater. A similar result was obtained in [14], where resistances to impact of thin strings and membranes (respectively, plane and axisymmetric cases) were compared.

Normal stresses $\sigma_{zz}(r,0)$ vs. time at the interface $r \le r^*$ shown in Figs. 6 and 7 were calculated for conical punches. The problem formulation corresponds to the case when the external loading (normal velocity) appears at the moment $t = 0$ at point $(0,0)$ and then moves along the surface $z = 0$ with a constant speed determined by the cone opening. Let the half of the cone opening be φ (geometrical schemes are located in the left of the shown σ_{zz} pictures), then the front speed of the moving loading is $V^* = \operatorname{tg}\varphi$, and $V_0(r,t) =$ $= H(r - V^*t)$.

Calculation examples shown in Fig. 6 correspond to supersonic velocities V^*: $V^* = \operatorname{tg}\varphi = 2$ (the left column) and $V^* = \operatorname{tg}\varphi = 4$ (the right column). Results in Figs. 6*a* and 6*b* are related to conical indenters unbounded in the radial direction (recall, the unbounded paraboloid indenter is referred in Fig. 2). Because in the considered case the continual problem has no length and time sizes, the mesh parameters Δx and Δt ($\Delta x = \Delta t = 0.01$) were taken as measurement units. In according with this, curves correspond to $r/\Delta x = 0, 10, 25, 50$, $100, 200$ and 400. Presented results show the detectable influence of the singular point $r = 0$: stresses at the interface possess constant amplitudes equal to 1 up to the moment of incoming of waves propagated from this singular point. Once after that, stresses increase with time, while their growth rate decreases with the distance from the axis. The smaller the cone opening, the more distinctly the described process is revealed.

Stresses $\sigma_{zz}(r,0)$ depicted in Figs. 6*c* and 6*d* are calculated in the case of combined cylindrical indenters ($R = 1$) with conical heads indented into a half-space; curves correspond to $r = 0, 0.25, 0.5, 0.9, 0.95, 0.99$ and 1.00. The main characteristic of the process is that the wave picture is formed by stresses induced from two singular points $r = 0,\ z = 0$ and $r = 1,\ z = 0$. The influence of the more sharp singularity at $r = 1$ prevails with time, and the stress pattern is approached to that obtained in the case of a plane head punch.

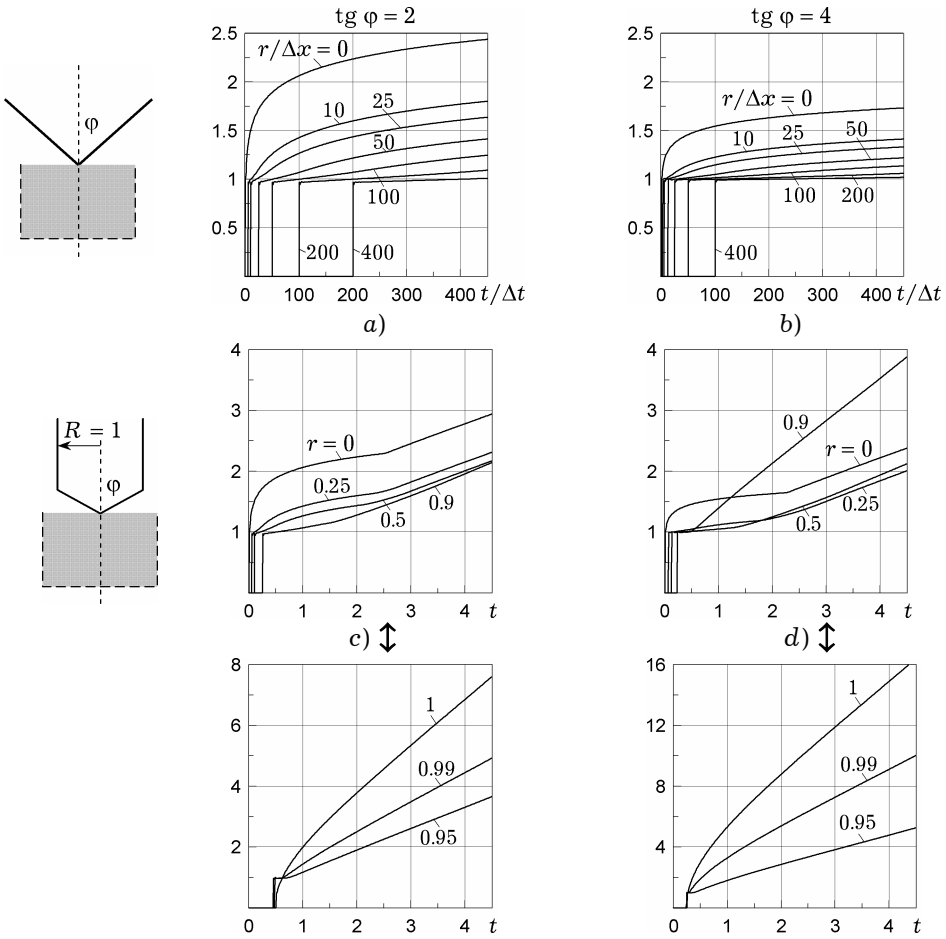

Fig. 6. Conical and combined indenters vs. an elastic halfspace: *a*), *b*) unbounded cones, curves correspond to $r/\Delta x = 0, 10, 25, 50, 100, 200$, and 400; *c*), *d*) cylindrical indenter with conical heads, curves correspond to $r = 0, 0.25, 0.5, 0.9$, $0.95, 0.99$ and 1.00.

Results shown in Fig. 7 are calculated in the case $\operatorname{tg}\varphi = 2$. Curves depicted in Fig. 7*a* correspond to interaction of an unbounded conical indenter with a layer of thickness $h = 1$. As above, in Figs. 6*a* and 6*b*, curves correspond to $r = 0, 0.1, 0.25, 0.5, 1.0, 2.0$ and 4.0. It can be seen that the stress pattern remains the same that in the previous case up to incoming the first reflection from the backing to singular point $r = 1$, $z = 0$. One can see «spreading fronts» of first reflections at the region adjacent to the axis, where the relative contribution to the general pattern is more significant of waves induced from singular point $r = 0$, $z = 0$. This contribution increases with t and r, as the described values are approached to the step-change character inherent the simplest one-dimensional case when $\varphi \to \pi/2$.

Stresses shown in Fig. 7*b* are calculated in the case of indentation into a layer ($h = 1$) of the cylindrical punch ($R = 1$) with the conical head; curves correspond to $r = 0, 0.25, 0.5, 0.9, 0.95, 0.99$ and 1.00. In the region adjacent to the axis (curves for $r = 0, 0.25, 0.5$ and 0.9) the influence is observed of converged shear waves induced by the singular point $r = 1, z = 0$, while the most influence of this singularity is detected in the nearest vicinity of the edge (curves for $r = 0.95, 0.99$ and 1.00). The action of reflected waves is qualitatively the same as in the case of a plane indenter head.

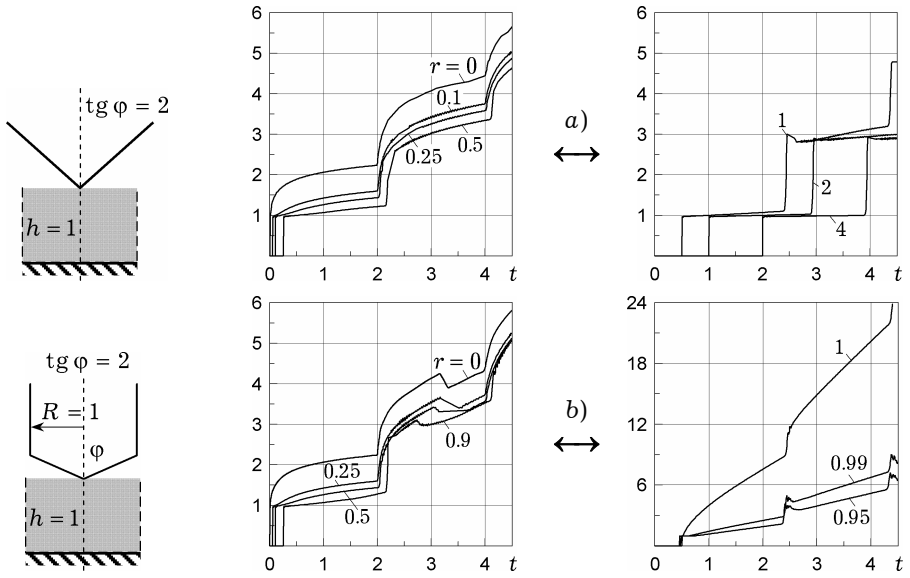

Fig. 7. Conical and combined indenters vs. a layer: *a*) unbounded cone, curves correspond to $r = 0, 0.1, 0.25, 0.50, 1.00, 2.00$ and 4.00 (these value are the same as in Fig. 6*a*, *b*); *b*) cylindrical indenter with a conical head, curves correspond to $r = 0, 0.25, 0.5, 0.9$, $0.95, 0.99$ and 1.00 (these value are the same as in Fig. 6*c*).

The last group of results (Figs. 8, 9) show stresses at the interface and peculiarities of the motion pattern of plane face cylindrical punches of various masses indented into a halfspace. The upper row of pictures in Fig. 8 ($M = 2.5$, $5.0, 10.0$; the punch mass is normalized by value $\pi\gamma R^3$) shows normal stresses $\sigma_{zz}(r,0)$ at the interface vs. time; curves correspond to $r = 0, 0.5, 0.75, 0.9$ and 0.95, while stresses $\sigma_{zz}(1,0)$ are depicted in Fig. 9; curves correspond to $M =$ $= 1.0, 2.5, 5.0, 10, 100, \infty$.

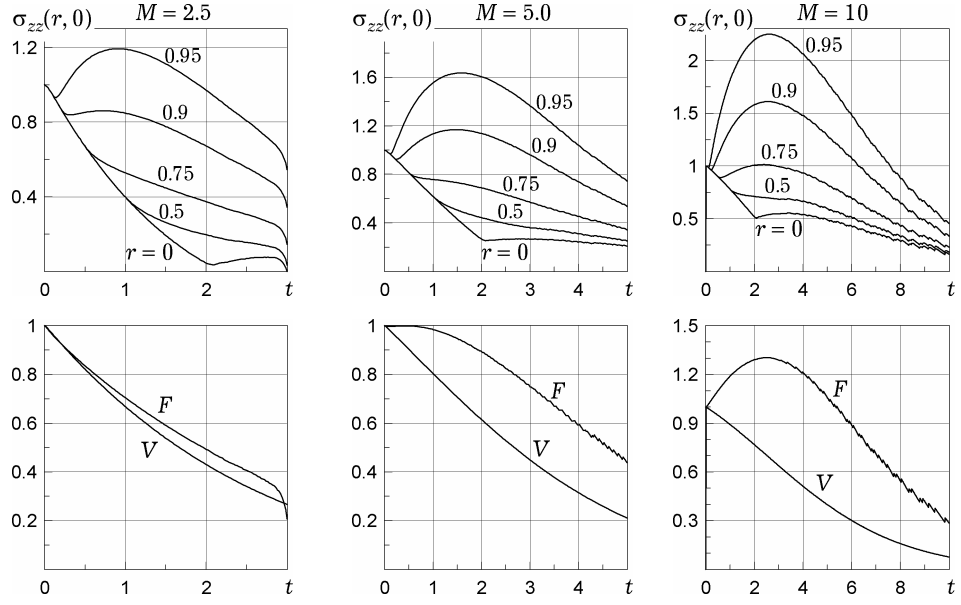

Fig. 8. Finite mass cylindrical indenters with a flat head vs. an elastic halfspace: normal stresses $\sigma_{zz}(r,0)$ vs. time, curves correspond to $r = 0, 0.5, 0.75$ 0.9 and 0.95 (upper row); drag F and punch indentation velocity V vs. time (lower row).

Drag F and punch indentation velocity V vs. time are depicted in the low row of Fig. 8. The calculation process is restricted by time moment $t = t_{\text{ext}}(M)$ when an extension in interface $z = 0$ is detected. In presented examples the following values t_{ext} are obtained: $t_{\text{ext}} = 3.03$ $(M = 2.5)$, $t_{\text{ext}} = 4.96$ $(M = 5)$ and $t_{\text{ext}} = 9.36$ $(M = 10)$.

At the process beginning ($t = \Delta t$ in the discrete model) we, as expected, obtain: $\sigma(r,0) = V = 1$, $F = 1$. Once after that the punch speed monotonically decreases up to the time moment $t_r = 2(1 - r)$ when shear waves radiated by edge $R = 1$ are detected in current section r. In this moment, a kink is appeared in curve $\sigma(r,0)$ resulting in deceleration of stresses decreasing at the axis vicinity and, vice versa, in stresses increasing at the edge vicinity. In the latter, stresses reach the maximal value, which increases with M; the drag is changed by the similar way.

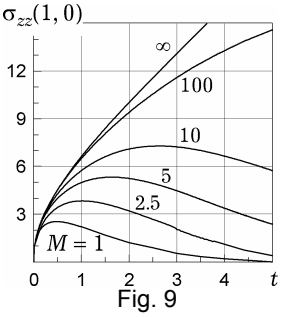

Fig. 9

Finally we tentatively evaluate dimensional impact velocities correctly determined by using linear theory of elasticity. Following to Fig. 9 we obtain maximal values of strains at interface $z = 0$: $(\varepsilon_{zz})_{\max} \sim (2.5, 4, 5.3, 7.5, 15)\ V_0/c_p$. Let $c_p = 5000$ m/s. Let also the linearity condition be violated if $\varepsilon_{zz} \geq 0.005$. Then to ensure that linear theory of elasticity is consistent, inequalities $V_0 \leq$ $\leq (3.3, 6.9, 9.9, 13.4$ and $21.1)$ m/s can be proved for $M = 100, 10, 5, 2.5$ and 1.0 correspondingly.

Obtained results can be summarized by the following conclusions:

- An analytical solution of the considered problem was built in the case of blunt solid body indented with a constant velocity into an elastic layer.
- Numerical algorithms to problem solving have been designed on the basis of the MDM technique. The computer solution allows step-wise character of the wave process to be precisely revealed.
- Parametric analysis of the problem was conducted for a set of indenter shapes and mass values. The emphasis is made to development of the stress pattern in cases of singular shapes of the indenter head.

Acknowledgements: This research was supported by the Israeli Science Foundation, Grant No. 504/08. The first author is indebted to Prof. Miriam Cohen, director of the Center of Advanced Studies of Mathematics at Ben-Gurion University of the Negev, for the opportunity to complete this collaboration work at the BGU Department of Mathematics.

1. *Abdukadyrov S. A., Pinchukova N. I., Stepanenko M. V.* A numerical approach to solving dynamic equations of elastic media and structures // Sov. Mining Sci. – 1984. – **21**, No. 6. – P. 34–41.
2. *Abdukadyrov S. A., Pinchukova N. I., Stepanenko M. V.* Nonstationary diffraction of plane longitudinal wave on an elastic cylindrical shell // Mechanics of Solids. – 1989. – **24**, 5. – P. 136–142.
3. *Ayzenberg-Stepanenko M. V., Sher E. N.* Modeling wave processes in periodic structures // J. Phys. Mesomech. – 2007. – **1**. – P. 34–43.
4. *Bajer A., Demkowicz L.* Dynamic contact/impact problems, energy conservation, and planetary gear trains // Comput. Meth. Appl. Mech. and Eng. – 2002. – **191**, No. 37–38. – P. 4159–4191.
5. *Gordienko V. I., Kubenko V. D., Stepanenko M. V.* Effect of a nonstationary internal wave on an elastic cylindrical shell // Soviet Appl. Mech. – 1981. – **17**, No. 3. – P. 245–249.
6. *Kubenko V. D.* Impact of blunted bodies on a liquid or elastic medium // Int. Appl. Mech. – 2004. – **40**, No. 11. – P. 1185–1225.

7. *Kubenko V. D., Ayzenberg-Stepanenko M. V.* Impact indentation of a rigid body into elastic layer. Analytical and numerical approaches // Мат. методи та фіз.-мех. поля. – 2008. – **51**, № 2. – С. 61–74.
8. *Kubenko V. D., Marchenko T. A.* Nonstationary indentation of a rigid blunt indenter into an elasic layer: a plane problem // Int. Appl. Mech. – 2008. – **44**, No. 3. – P. 286–95.
9. *Maekava I.* Size effect of impact strength and related applications // Size scale effects in the failure mechanisms of materials and structures / Ed. A. Carpenteri. – London: E&FN SPONS, 1996. – P. 567–573.
10. *Maekava I.* The influence of stress wave on the impact fracture strength of cracked member // Int. J. Impact Eng. – 2005. – **24**. – P. 1–4.
11. *Mechanics* of contact interactions / Eds. I. I. Vorovich and V. M. Aleksandrov. – Moscow: Fizmatlit, 2001. (In Russian: *Механика* контактных взаимодействий / Под ред. И. И. Воровича, В. М. Александрова. – Москва: Физматлит, 2001. – 670 с.)
12. *Rakhamatullin H. A.* On propagation of elastic-plastic waves in a halfspace // Appl. Math. Mech. – 1959. – **23**. – P. 79–86.
    Рахматулин Х. А. О распространении упруго-пластических волн в полупространстве // Прикл. математика и механика. – 1959. – **23**. – С. 419–424.
13. *Slepyan L. I., Ayzenberg-Stepanenko M. V.* Localized transition waves in bistable-bond lattices // J. Mech. Phys. Solids. – 2004. – **52**. – P. 1447–1479.
14. *Slepyan L. I., Ayzenberg-Stepanenko M. V.* Penetration of metal-fabric composites by small projectiles // Personal Armor Systems. – London: British Crow Copyright, 1998. – P. 289–298.
15. *Stepanenko M. V.* Computing the pulsed strain processes in elastic structures // Sov. Mining Sci. – 1976. – **12**, No. 2. – P. 53–57.
16. *Wang F.-J., Wang L.-P., Cheng J.-G., Yao Z.-H.* Contact force algorithm in explicit transient analysis using finite-element method // Finite Elements in Analysis and Design. – 2007. – **43**, No. 6-7. – P. 580–587.
17. *Zhong Z.-H., Mackerie J.* Contact-impact problems: A review with bibliography // Appl. Mech. Rev. – 1994. – **47**, No. 2. – P. 55–76.

УДАРНЕ ВДАВЛЮВАННЯ ТВЕРДОГО ТІЛА В ПРУЖНИЙ ШАР. ОСЕСИМЕТРИЧНА ЗАДАЧА

Розглядається осесиметрична задача про нормальне вдавлювання твердого тіла в шар з пружного матеріалу. Точний аналітичний розв'язок задачі одержано у випадку вдавлювання із заданою швидкістю затупленого індентора, що супроводжується багатократними відбиттями хвиль від границь шару. Чисельний розв'язок задачі для індентора достатньо загального вигляду отримано на основі спрощеної моделі теорії пружності, в якій зберігається одне переміщення уздовж напрямку удару. Застосований явний скінченнорізницевий алгоритм базується на техніці мінімізації чисельної дисперсії. Наведено аналіз напруженого стану шару в залежності від часу, форми проникаючого тіла і його маси.

УДАРНОЕ ВДАВЛИВАНИЕ ТВЕРДОГО ТЕЛА В УПРУГИЙ СЛОЙ. ОСЕСИММЕТРИЧНАЯ ЗАДАЧА

Рассматривается осесимметричная задача о нормальном вдавливании твердого тела в слой из упругого материала. Точное аналитическое решение получено для случая вдавливания с заданной скоростью затупленного индентора, что сопровождается многократными отражениями волн от границ слоя. Численное решение задачи для индентора достаточно общего вида получено на базе упрощенной модели теории упругости, сохраняющей одно перемещение вдоль направления удара. Примененный явный конечно-разностный алгоритм базируется на технике минимизации численной дисперсии. Представлен анализ напряженного состояния слоя в зависимости от времени, формы проникающего тела и его массы.

[1] Timoshenko Inst. of Mechanics of NAS of Ukraine, Kiev,
[2] Ben-Gurion Univ. of the Negev, Be'er-Sheva, Israel

Received 04.03.09